Hindawi
International Journal of Antennas and Propagation
Volume 2019, Article ID 4074862, 9 pages
https://doi.org/10.1155/2019/4074862

Research Article

Microwave Tomography System for Methodical Testing of Human Brain Stroke Detection Approaches

Ilja Merunka,[1] **Andrea Massa**,[2] **David Vrba**,[3] **Ondrej Fiser**,[3] **Marco Salucci**,[2] **and Jan Vrba**[3]

[1]*Department of Electromagnetic Field, Czech Technical University in Prague, Prague, Czech Republic*
[2]*ELEDIA Research Center (ELEDIA@UniTN-University of Trento), Via Sommarive 9, I-38123 Trento, Italy*
[3]*Department of Biomedical Technology, Czech Technical University in Prague, Prague, Czech Republic*

Correspondence should be addressed to Ilja Merunka; merunilj@fel.cvut.cz

Received 19 October 2018; Revised 16 January 2019; Accepted 23 January 2019; Published 31 March 2019

Guest Editor: Sandra Costanzo

Copyright © 2019 Ilja Merunka et al. This is an open access article distributed under the Creative Commons Attribution License, which permits unrestricted use, distribution, and reproduction in any medium, provided the original work is properly cited.

In this work, a prototype of a laboratory microwave imaging system suitable to methodically test the ability to image, detect, and classify human brain strokes using microwave technology is presented. It consists of an antenna array holder equipped with ten newly developed slot bowtie antennas, a 2.5 D reconfigurable and replaceable human head phantom, stroke phantoms, and related measuring technology and software. This prototype was designed to allow measurement of a complete S-matrix of the antenna array. The reconfigurable and replaceable phantom has currently 23 different predefined positions for stroke phantom placement. This setting allows repeated measurements for the stroke phantoms of different types, sizes/shapes, and at different positions. It is therefore suitable for large-scale measurements with high variability of measured data for stroke detection and classification based on machine learning methods. In order to verify the functionality of the measuring system, S-parameters were measured for a hemorrhagic phantom sequentially placed on 23 different positions and distributions of dielectric parameters were reconstructed using the Gauss-Newton iterative reconstruction algorithm. The results correlate well with the actual position of the stroke phantom and its type.

1. Introduction

Microwave tomography (MWT) is an emerging imaging technique for retrieving the spatial distribution of dielectric parameters of biological tissues [1].

In microwave imaging, the imaged area is typically exposed to electromagnetic (EM) waves radiated by antenna(s) positioned around the imaged area. The spatial distribution of the dielectric parameters in the imaged area influences the way of propagation of these waves, and the resulting EM field is subsequently measured by the same antennas. The measured data is used to estimate the distribution of dielectric properties within the imaged area.

While the use of nonionizing radiation in MWT systems is a good argument when looking for benefits over a computed tomography and mammography (nonionizing radiation would allow frequent screenings), portability and cost effectiveness are good points when comparing MWT with magnetic resonance imaging [2].

Although one of the first reference of microwave hemorrhagic stroke detector can be found in the US patent by inventors Haddad and Trebes [3], there are nowadays several research groups working towards early stroke detection and differentiation systems. Just to name few leaders of the groups active in this field—Mikael Persson from Medfield Diagnostics AB, Sweden [4], Serguei Semenov from EMTensor GmbH, Austria [5], Amin Abbosch from The University of Queensland, Australia [6], and Lorenzo Crocco from the National Research Council of Italy, Italy [7–9]. Thorougher review can be found in [10].

In general, two different approaches for detection and classification of strokes can be found in literature: methods

based on visualization (image reconstruction) of dielectric parameters distribution in the region of interests [6, 11] and methods based on machine learning algorithms [4, 12, 13].

Most of the published systems (both hardware and reconstruction/classification algorithms) have not been systematically tested. Typically, one or two stroke phantom positions are selected, and the results obtained are evaluated and presented.

In this paper, we designed and tested a laboratory microwave imaging system suitable for measuring head and stroke phantoms of various types, shapes, and sizes. The stroke phantoms could be placed at any of 23 predefined positions covering almost all the volume of the head phantom. Such a system is especially suited for testing methods for stroke detection and classification based on machine learning algorithms, but it can be used for testing image reconstruction methods as well. Additionally, the proposed system allows testing of the two approaches for phantoms of different complexities and matching liquids of various dielectric properties. The system was tested using a simple 2.5 D reconfigurable head phantom with hemorrhagic stroke phantom, which was sequentially placed at some of the predefined positions. The system, phantoms, and measurements are described in Section 2. Section 3 includes an analysis of the measured data as a function of stroke phantom position. Finally, a deterministic iterative algorithm for the reconstruction of the dielectric properties distribution was applied in Section 4 to the measured data in order to verify functionality of the presented system.

2. Microwave Imaging System Description

2.1. Phantoms of Head and Brain Strokes, Antenna Array. The shape of the head phantom was designed with respect to the main objective of the article, namely, to systematically test the use of microwave imaging for the purpose of detection and classification of brain strokes occurring anywhere in the volume of human brain. For this, it is necessary to be able to place a stroke phantom on a predefined position in the entire head phantom. Towards this end, a liquid head phantom has been chosen to fill an elliptical container with a human head-shaped cross section in a transverse plane. The head phantom vessel is placed into the antenna element holder. The space between the vessel and the holder is filled with a matching liquid, see Figure 1. Both the antenna holder and the head phantom vessel have a height of 200 mm (including a base of 4 mm) and a wall thickness of 2 mm. The numerical model of the proposed system and its physical form are shown in Figure 2. 23 octagonal pins are designed at the bottom of this container and are used to define the positions of phantoms of strokes. These latter are made by hollow cylinders filled by liquids of desired dielectric parameters, having an octagonal opening in their bottom. This ensures accurate and repeatable placement of phantoms of strokes in the head phantom. The containers for stroke phantoms have an internal diameter of 40 mm, a height of 196 mm, and a wall thickness of 1 mm. All the parts were made by 3D printing using Prusa i3 MK2 (Prusa Research, Czech Republic) and PETG material.

2.2. Antenna Elements. Ten identical slot bowtie antennas (antenna design is described in [14]) were placed on the walls of the antenna array holder. The antennas were made of two layers of 1.5 mm RF substrates Rogers R04003C with the dimensions of 59×59 mm^2 and realized by Pragoboard s.r.o., Prague, Czech Republic. The main advantages of this antenna element design are suppressed radiation outside the imaging area, symmetry of radiated field, mechanical stiffness, and easy, inexpensive, and repeatable production. The front side of the realized antenna and the modules of measured reflection coefficients of all 10 antenna elements laid on the surface of a liquid head phantom are illustrated in Figure 3. The reflection coefficients of all ten antenna elements show virtually identical values and a low amplitude (less than -10 dB) in the frequency range from nearly 0.9 to 1.3 MHz. The system introduced in this work can therefore be used at any frequency in this frequency band. The frequency band was chosen in view of the fact that it fits into frequency bands already considered the most suitable for this application [7] considering attenuation of EM waves inside the human head and resolution of the imaging method. Although the authors believe that the higher number of antennas would lead to better results, the maximal number of antennas is determined by the actual dimensions of the container and the used antenna elements.

2.3. Measurement Setup and Settings. The measuring instruments used in the presented MWI system are the microwave switching matrix ZN-Z84-B42 (Rohde & Schwarz, Germany) and the vector network analyzer (VNA) ZNB4-B32 (Rohde & Schwarz, Germany). The antennas were connected to the switching matrix test ports using semirigid coaxial cables (Rohde & Schwarz, Czech Republic). Although the isolation between all tested matrix ports should be greater than 90 dB, 10 out of 24 ports of the switching matrix test ports involved in the measurement were selected for the highest possible isolation between channels. The fact that 90 dB isolation should be sufficient is supported by another group that used an 80 dB [4] custom-made switching matrix. All high-frequency connections were tightened by a torque wrench 0.9 Nm. Setting and triggering of measurements together with reading out of the measured data were done with MATLAB scripts written in-house (MathWorks, MA, USA). The photograph of the MWI system is shown in Figure 2. The following parameters of the measurement instruments were used: operating frequency 1 GHz, intermediate frequency bandwidth 30 Hz, and output power of the VNA 13 dBm. The working frequency 1 GHz was selected with respect to penetration depth, spatial resolution, and last but not least the fact that it fits into the frequency interval preferred for the same application in [7].

2.4. Calibration. A full-port calibration was performed just before the measurement using the automatic calibration unit ZN-Z153 (Rohde & Schwarz, Germany).

Throughout the calibration period, the antenna elements were disconnected from the coaxial cables leading into the switching matrix. To these open ends of the coaxial cables,

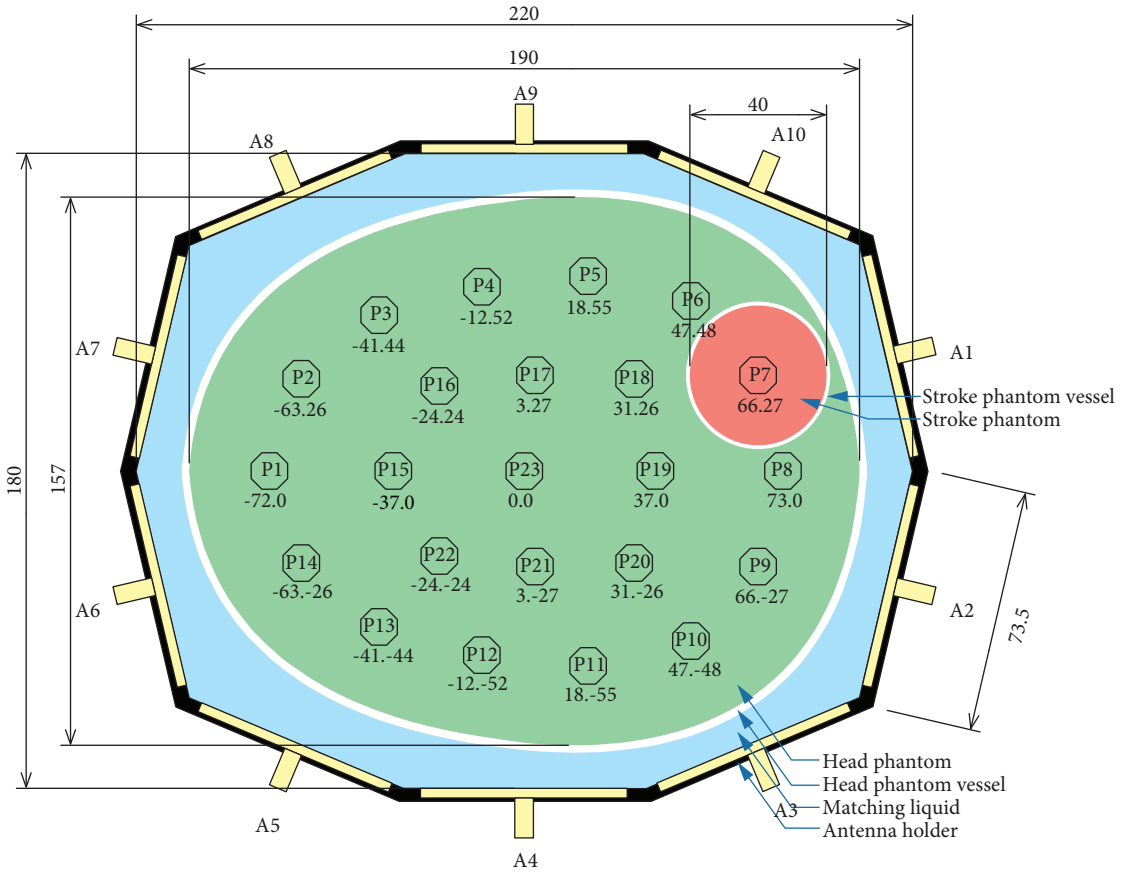

Figure 1: Bottom view of measuring container with marked positions of the stroke phantoms. Black: walls of the antenna holder, yellow: antennas with ports, blue: matching liquid, white: head phantom vessel, green: liquid phantom of human head, and red: liquid phantom of stroke at position P7 (all dimensions are in mm).

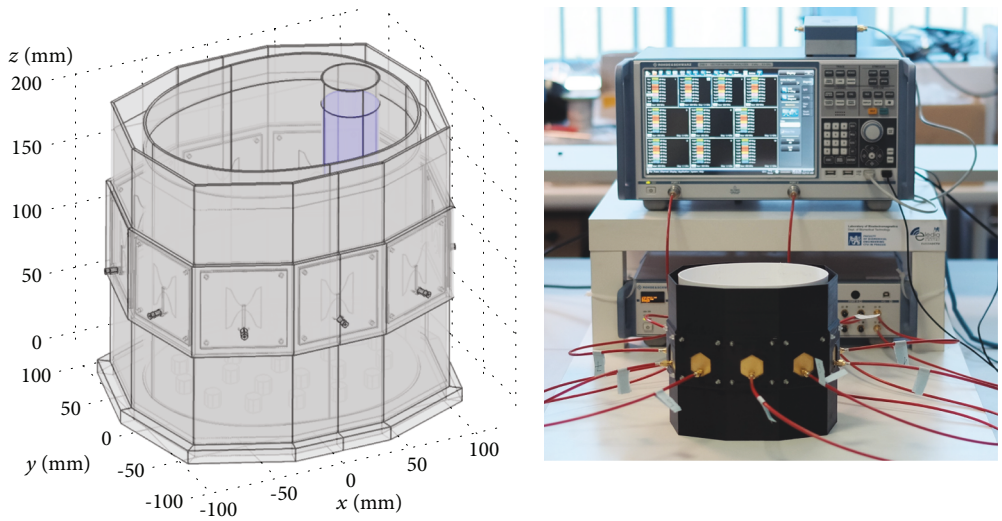

Figure 2: 3D model of measuring container with antennas and cylindrical phantom of stroke marked blue (a) and the photograph of the measuring setup (b).

the calibration unit was three times reconnected (due to the lower number of ports of the calibration unit than the number of used antenna elements/system channels) following the calibration instructions displayed on the VNA. In this way, the switching matrix was included in the full-port VNA calibration.

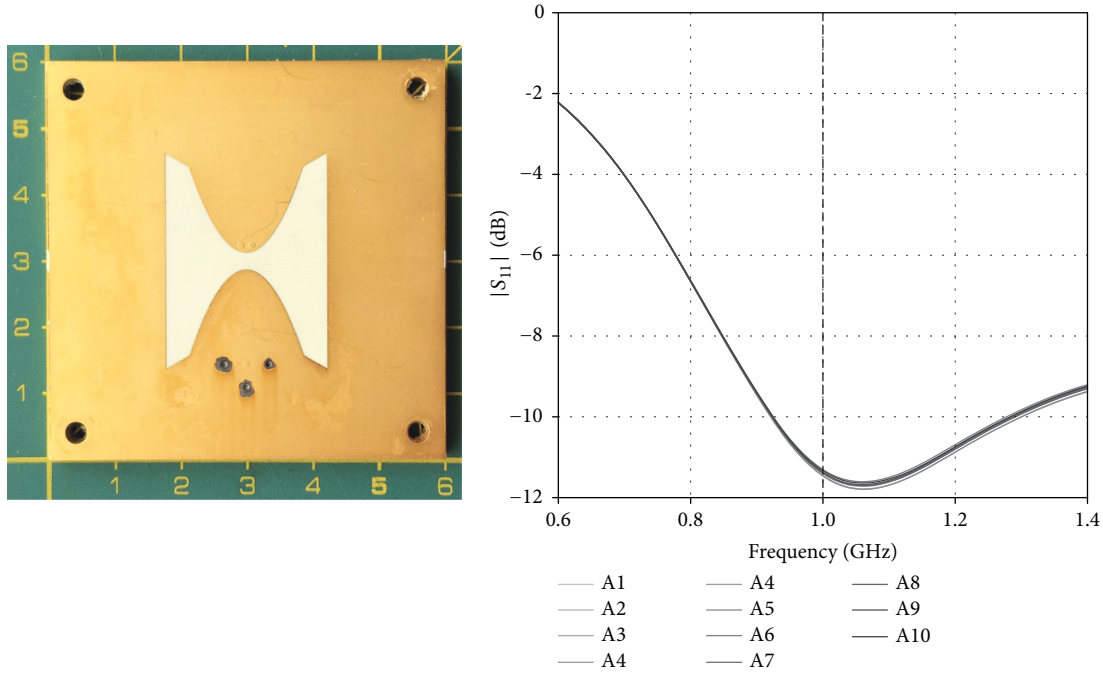

(a) (b)

Figure 3: Photograph of the antenna element from the side facing to the phantom (a) (dimensions in cm) and measured magnitude of S_{11} for all antennas in frequency range 0.6 - 1.4 GHz heading to the liquid homogeneous phantom of human head (b). Central operating frequency is marked by a dashed line.

The VNA, switching matrix, and automatic calibration unit were turned on 90 minutes before the calibration onset. Calibration data was saved and reloaded before each measurement.

2.5. Liquid Phantom Composition and Dielectric Properties. Two liquid phantoms substituting healthy head and brain hemorrhagic stroke tissue were prepared. The dielectric properties of the head phantom are equal to average dielectric parameters of a human head ($\varepsilon_{r,HH} = 39.8$, $\sigma_{HH} = 0.94$ S/m) [15]. The dielectric properties of the hemorrhagic stroke phantom are chosen based on the knowledge of the dielectric properties of blood [16], where the contrast to brain tissues is about 50 - 60%. A conservative change at the level of 30% is chosen here ($\varepsilon_{r,HR} = 51.4$, $\sigma_{HR} = 1.22$ S/m) as in [5]. Dielectric properties of the phantoms were measured using DAK (Schmid & Partner Engineering AG, Switzerland) just before the measurement in the MWI system prototype. Compositions in weight percent and comparison of target and measured dielectric properties of the phantoms are listed in Table 1. In this table, the HEAD marks the column devoted to the phantom of the head and the HEM marks the column devoted to the hemorrhagic stroke phantom. The dielectric parameters listed in rows following the compositions were measured at a frequency of 1 GHz and 25°C before the measurement in the MWI system. In order to eliminate the reflections from the interface matching liquid-head, the head phantom material was also used as the matching liquid between the antennas and the head vessel.

Table 1: Phantom composition in weight percent, target, and measured dielectric parameters at 1 GHz and 25°C, immediately before the measurement in the MWI system.

	HEAD	HEM
Isopropyl alcohol (wt%)	50.48	34.00
Deionized water (wt%)	48.35	64.67
NaCl (wt%)	1.16	1.33
Target ϵ_r (-)	39.60	51.48
Measured ϵ_r (-)	39.80	51.37
U ($k = 2$) (%)	1.7	2.1
Target σ (S/m)	0.94	1.220
Measured σ (S/m)	0.94	1.224
U ($k = 2$) (%)	2.7	2.7

U: expanded uncertainty of type B, HEAD: head phantom, HEM: hemorrhagic phantom.

2.6. Measuring Procedure. The antenna array holder and the head phantom vessel were firstly filled with homogeneous head phantom liquid. Special attention was paid to elimination of bubbles which appeared on the surface of antennas during the filling procedure of the container. Finally, the container was enclosed by microwave pyramid absorbers. The measurement procedure is composed from two main steps: (1) measurement of the MWI system filled with the head phantom only and (2) measurement with the head phantom including the hemorrhagic stroke phantom. The phantom of stroke was subsequently positioned and measured in all 23 positions (Figure 1). Whole S-matrix was measured 10 times

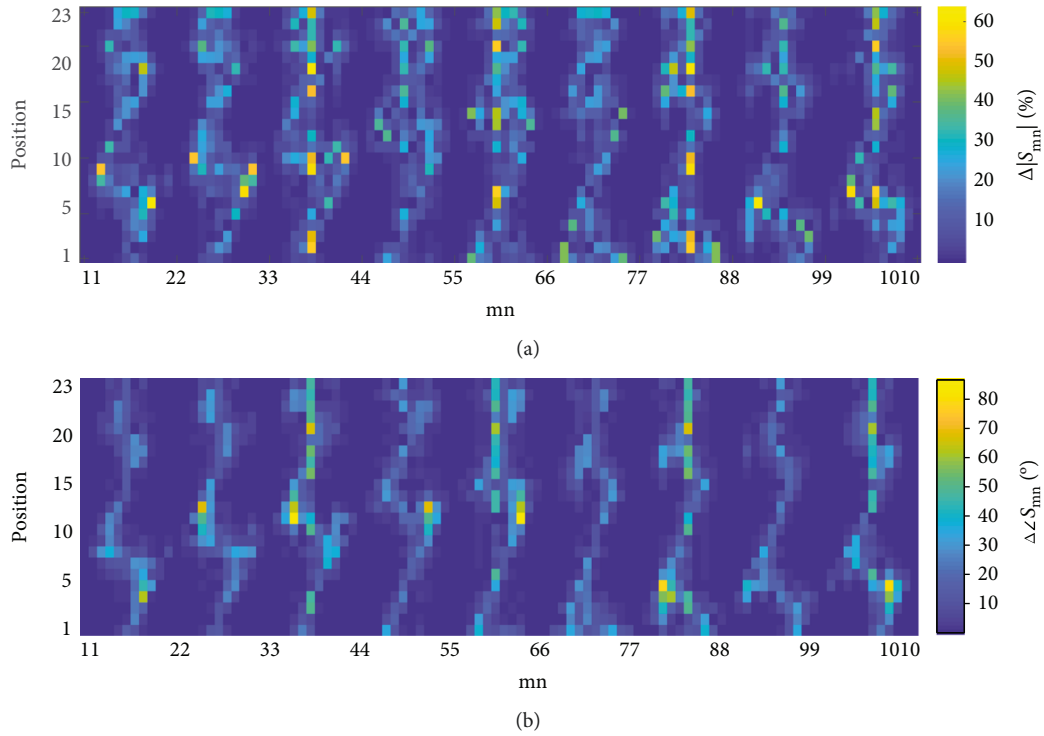

Figure 4: Response of the system ((a) relative change in the modulus of S-matrix and (b) change in the phase of S-matrix in degrees) to a presence of the hemorrhagic stroke phantom at 23 different positions (y axes) in the phantom of human head.

in series to cover fluctuations that could appear during the measurement for every position of the stroke. One measurement of the full S-matrix took about 12 s.

3. Measured Data

The response of the system to a presence of the phantom of hemorrhagic stroke at all 23 positions is visualized in Figure 4. It is calculated as the relative difference in the modules (equation (1)) and as the absolute difference in the arguments (equation (2)) of the S-parameters measured with (S_{mn}^{STROKE}) and without (S_{mn}^{HOMO}) the stroke phantom, respectively

$$\Delta|S_{mn}| = \frac{\left||S_{mn}^{STROKE}| - |S_{mn}^{HOMO}|\right|}{|S_{mn}^{HOMO}|}, \quad (1)$$

$$\Delta\angle S_{mn} = \left|\angle S_{mn}^{STROKE} - \angle S_{mn}^{HOMO}\right|. \quad (2)$$

The most responding S-parameters to the stroke at the specific position can be deduced from those images. The characteristic patterns in both amplitude and phase images indicate the strongest responses in transmission coefficients.

4. Application of Image Reconstruction Algorithm to Measured Data

A reconstruction algorithm based on Gauss-Newton algorithm with Tikhonov regularization [17] was used to reconstruct the dielectric image in the central plane of the antennas from the measured S-parameters. This algorithm is based on deterministic optimization procedure, assuming linear behavior of outcome in every iteration when only a small change in dielectric properties is introduced. In order to reduce the building time of the Jacobian matrix, the so-called adjoint method was used [18]. The value of the Tikhonov parameter was determined using the procedure described in [17].

4.1. Image Reconstruction Procedure. The image reconstruction procedure includes solution of forward problem (computation of electromagnetic field distribution and S-matrix), extraction of E-fields and S-matrix, computation of Jacobian, and computation of step in dielectric properties of the material domains. To model the propagation of E-field in the forward step, the 3D numerical version of the real measuring system was modeled in COMSOL Multiphysics (Figure 2(a)). Models of the real antennas together with SMA ports were used in the numerical model. Special attention was payed to correctly discretize all the model components. Finally, EM field was computed using the finite element method in 3D. All three components of E-field were extracted and used in the inverse step. In order to precisely represent the real-world scenario, any special assumption either simplification in the computational procedure of EM field was not made. Therefore, the framework presented in this paper can be easily adapted to the other realistic scenario by simply replacing the numerical model. Computation of the forward problem is the most computationally extensive procedure and takes about 150 minutes for all 10 antenna ports on the current PC (i7-6700 - 3.4 GHz, 64 GB DDR4

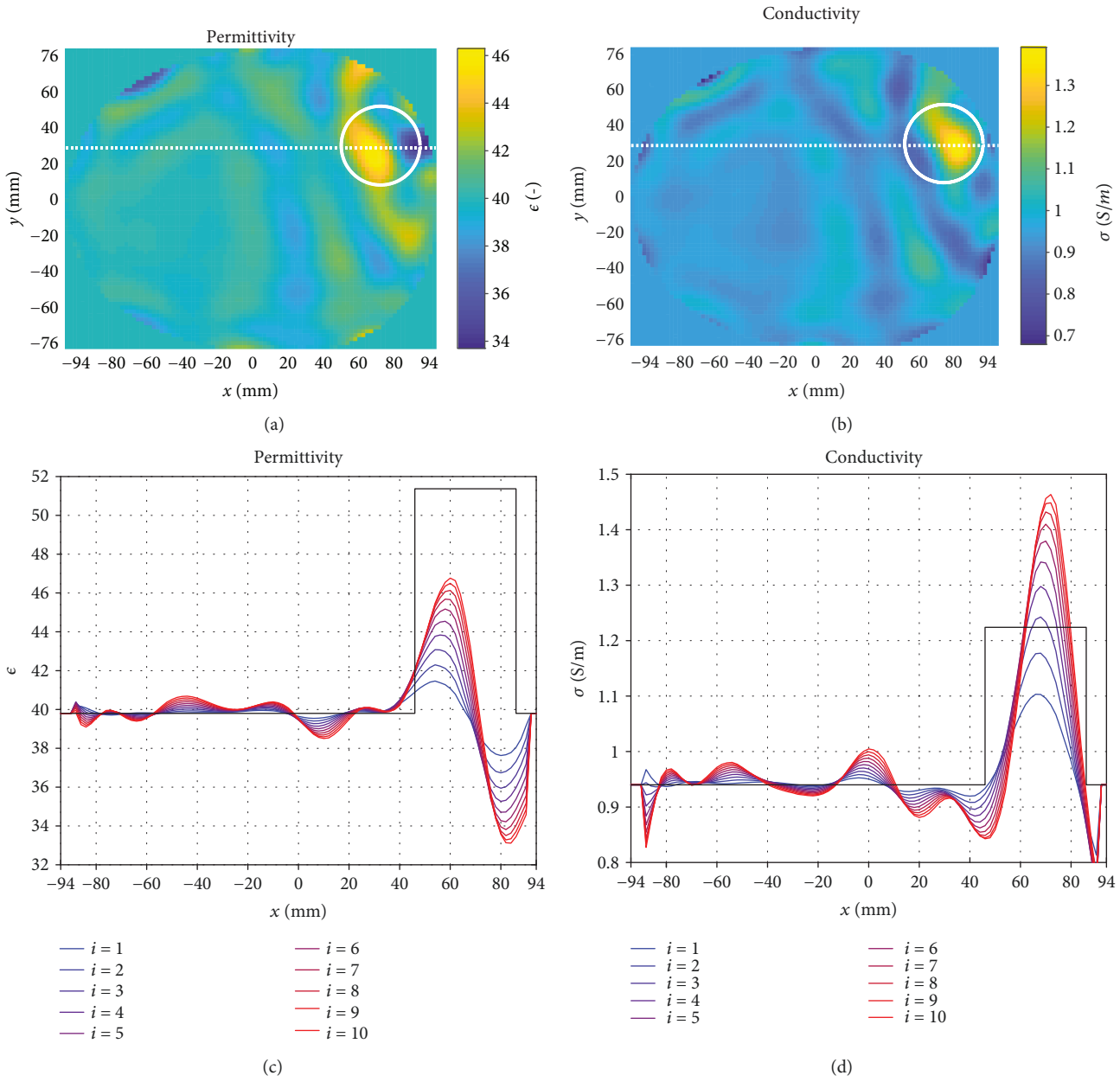

Figure 5: Results (a, b) of iterative reconstruction procedure for hemorrhagic stroke phantom at position P7 (marked by white circle) and evolution (c, d) of relative permittivity and conductivity over the iterations ($i = 1$ for the first iteration, $i = 10$ for the tenth iteration) on the line going through the center of the stroke phantom (marked by dashed white lines). Actual values of both relative permittivity and conductivity are marked by solid black lines in graphs (c) and (d).

RAM - 2133 MHz). The reconstruction algorithm was implemented in MATLAB.

In an attempt to achieve the actual values of complex permittivity in the region of interest, 10 iterations of the reconstruction algorithm were performed. Since the image reconstruction takes more than 25 hours for 10 iterations, the maximal number of iterations allowed was set to 10. Better results could be possibly achieved with higher number of iterations. However, as it can be seen from Figure 5, there is only a small change in the dielectric parameters over the last few iterations. Results of the reconstruction in a plane going through the center of the antennas for hemorrhagic stroke at position P7 are shown in Figure 5. Even though values of relative permittivity and conductivity in the reconstructed images did not reach the actual values and shape of the stroke, the biggest change in those quantities can be observed in the area of the stroke phantom (white circle).

Nine different unique positions of the stroke phantom inside the head phantom were selected, and the measured data were processed with the image reconstruction algorithm. In order to show the results of the reconstruction for all the positions of the stroke in one image, 350 values of relative permittivity and conductivity differing the most from the background matching liquid were detected in all

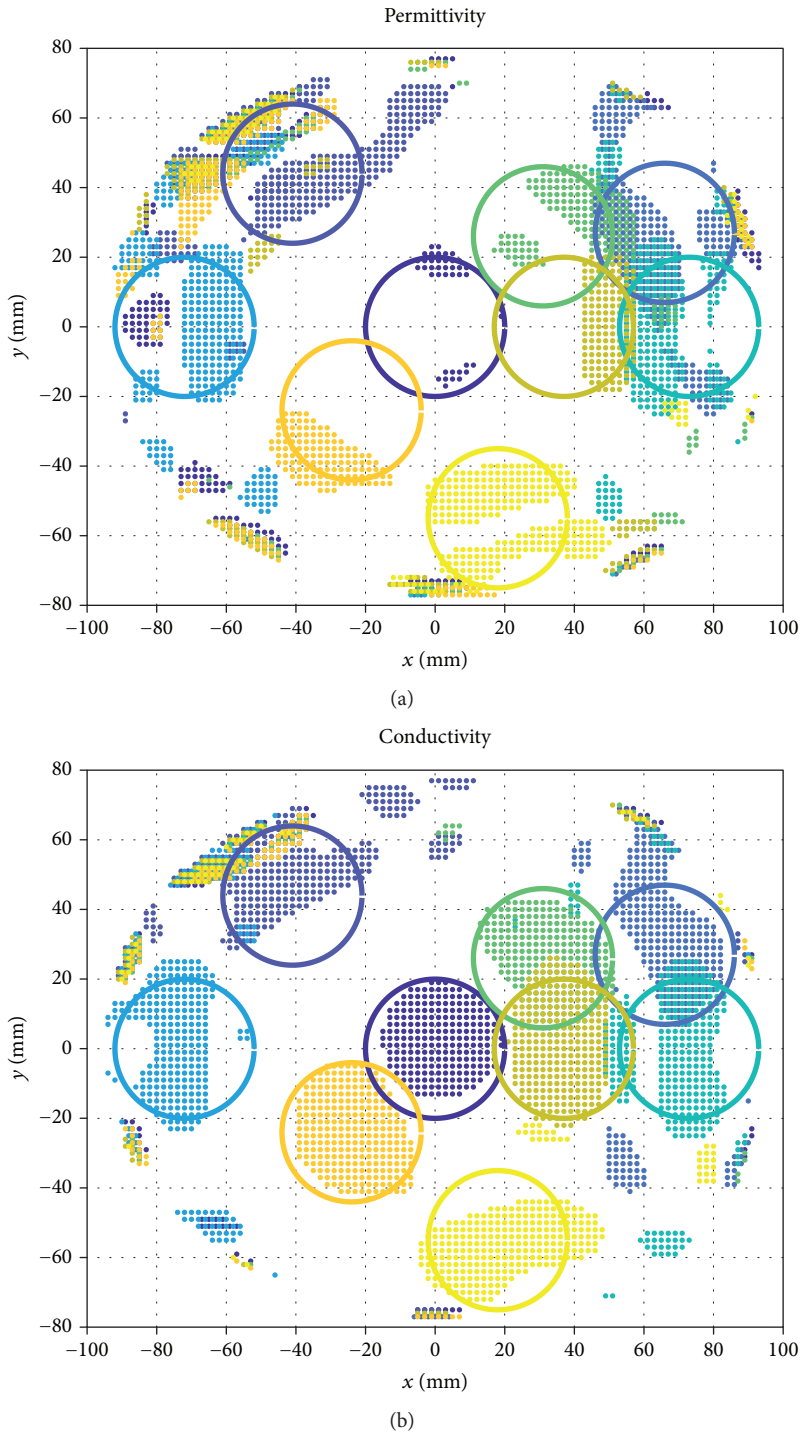

Figure 6: Detection of position of the strokes from reconstructed images. Circles mark the actual position of the stroke; dots of adequate color show the detected positions.

Table 2: Maximal values of dielectric parameters for the selected positions of the stroke phantom after the reconstruction.

Position	P1	P3	P7	P8	P11	P18	P19	P22	P23
max ϵ_r (-)	48.13	51.34	46.30	47.60	44.87	44.71	44.71	45.23	44.48
max σ (S/m)	1.42	1.32	1.39	1.38	1.30	1.23	1.24	1.22	1.24

9 images and its positions plotted together for every stroke phantom position, see Figures 6(a) and 6(b). In this figure, the threshold used to allow the binarization is based on the assumption that the size of the stroke phantom is known. And so, the size of the area covered by the dots of the specific color in Figure 6 is equaled to the size of the area of the cross-section of the stroke phantom. Positions of the stroke phantom can be better recognized from images depicting conductivity. Since the quantitative information is lost in Figure 6, the maximal values of dielectric parameters are listed in Table 2.

5. Discussion

The MWI systems are very sensitive to the quality of conducted microwave measurement. There are many cofounders, including temperature drift of measuring devices, changes in complex permittivity of phantoms due to the changes in temperature, evaporation and possible leak of liquids during stroke phantom replacement procedure, appearance of bubbles in the liquid phantoms, and quality of multiport calibration procedure, that the experimenter has to deal with during the measuring procedure. All those sources of noise negatively impact the quality of reconstructed images.

Conservative estimates of the differences between the dielectric properties of brain tissues and areas affected by strokes were considered. It can be assumed that a higher contrast in the dielectric properties of the head phantom and stroke phantoms would yield in better reconstruction results.

The number of antennas/channels of the presented system was determined by the dimensions of the human head/head phantom and the antenna element. For the used antenna elements, only limited size reductions can be achieved. Metamaterial-based structures such as described in [19–21] could be suitable for systems with a higher number of the antenna elements.

The forward problem in every iteration is solved for every antenna element. This can be done in parallel and thus reduce the total computational time. Further reduction of the computational time could be achieved by using the Finite Differences in Time-Domain Method (FDTD) which can be accelerated using GPU. If a broadband formulation of FDTD is used, it is possible to obtain results for multiple frequencies in a single simulation without a significant computational time increase.

In this work, imaging results for only 9 stroke phantom positions are presented, although there are in total of 23 positions available. This step is only motivated by the clarity of the imaging results presented. The 9 positions considered were carefully selected based on the geometric symmetry of the head phantom and antenna array. In other words, the imaging results for each of the remaining 14 positions would not differ much from the results corresponding to one of the 9 positions.

6. Conclusion

The prototype of the MWT system allowing systematic evaluation of human brain stroke detection and classification approaches has been presented in this paper. In order to prove the capabilities of the presented system, hemorrhagic phantom of human brain stroke was prepared and the experimental measurements were conducted with this stroke sequentially placed at 23 different positions in the head phantom. Achieved results support the statements of another groups working in this field that the detection and differentiation of the strokes by means of microwave technique should be possible at least in the laboratory conditions. In our future work, we are going to improve our system in several ways to deal with some major known issues such as low sensitivity, spatial resolution, and sensitivity to noise. A 2.5 D anatomically realistic head phantom consisting of three solid layers with shape and dielectric properties corresponding to skin, skull, and cerebrospinal fluid is currently under development. We also plan to combine the reconstructed images with detection and classification by algorithms of machine learning.

Data Availability

The data used to support the findings of this study are available from the corresponding author upon request.

Conflicts of Interest

The authors declare that there is no conflict of interest regarding the publication of this paper.

Acknowledgments

This work has been supported by a grant from the Czech Science Foundation, number 17-00477Y.

References

[1] A. Fhager, P. Hashemzadeh, and M. Persson, "Reconstruction quality and spectral content of an electromagnetic time-domain inversion algorithm," *IEEE Transactions on Biomedical Engineering*, vol. 53, no. 8, pp. 1594–1604, 2006.

[2] P. M. Meaney, "Microwave imaging and emerging applications," *International Journal of Biomedical Imaging*, vol. 2012, Article ID 252093, 2 pages, 2012.

[3] W. Haddad and J. Trebes, "Microwave hemorrhagic stroke detector," US Patent US20 030 018 244 A1, 2003, US Classification 600/371; International Classification A61B5/05; Cooperative Classification A61B5/4076, A61B5/0507, A61B5/05; European Classification A61B5/05M, A61B5/05, https://www.google.ch/patents/US20030018244.

[4] M. Persson, A. Fhager, H. D. Trefna et al., "Microwave-based stroke diagnosis making global prehospital thrombolytic treatment possible," *IEEE Transactions on Biomedical Engineering*, vol. 61, no. 11, pp. 2806–2817, 2014.

[5] M. Hopfer, R. Planas, A. Hamidipour, T. Henriksson, and S. Semenov, "Electromagnetic tomography for detection, differentiation, and monitoring of brain stroke: a virtual data and human head phantom study," *IEEE Antennas and Propagation Magazine*, vol. 59, no. 5, pp. 86–97, 2017.

[6] D. Ireland, K. Bialkowski, and A. Abbosh, "Microwave imaging for brain stroke detection using Born iterative method,"

IET Microwaves, Antennas & Propagation, vol. 7, no. 11, pp. 909–915, 2013.

[7] R. Scapaticci, L. Di Donato, I. Catapano, and L. Crocco, "A feasibility study on microwave imaging for brain stroke monitoring," *Progress In Electromagnetics Research B*, vol. 40, pp. 305–324, 2012.

[8] R. Scapaticci, O. M. Bucci, I. Catapano, and L. Crocco, "Differential microwave imaging for brain stroke followup," *International Journal of Antennas and Propagation*, vol. 2014, Article ID 312528, 11 pages, 2014.

[9] R. Scapaticci, J. Tobon, G. Bellizzi, F. Vipiana, and L. Crocco, "Design and numerical characterization of a low-complexity microwave device for brain stroke monitoring," *IEEE Transactions on Antennas and Propagation*, vol. 66, no. 12, pp. 7328–7338, 2018.

[10] L. Crocco, I. Karanasiou, M. L. James, and R. C. Conceição, Eds., *Emerging Electromagnetic Technologies for Brain Diseases Diagnostics, Monitoring and Therapy*, Springer International Publishing, 2018, https://www.springer.com/la/book/9783319750064.

[11] A. Abbosh, "Microwave systems for head imaging: challenges and recent developments," in *2013 IEEE MTT-S International Microwave Workshop Series on RF and Wireless Technologies for Biomedical and Healthcare Applications (IMWS-BIO)*, pp. 1–3, Singapore, December 2013.

[12] M. Salucci, J. Vrba, I. Merunka, and A. Massa, "Real-time brain stroke detection through a learning-by-examples technique - an experimental assessment," *Microwave and Optical Technology Letters*, vol. 59, no. 11, pp. 2796–2799, 2017.

[13] M. Salucci, A. Gelmini, J. Vrba, I. Merunka, G. Oliveri, and P. Rocca, "Instantaneous brain stroke classification and localization from real scattering data," *Microwave and Optical Technology Letters*, vol. 61, no. 3, pp. 805–808, 2019.

[14] I. Merunka, J. Vrba, O. Fiser, and D. Vrba, "Comparison of bowtie slot and rectangular waveguide-based antennas for microwave medical imaging," in *12th European Conference on Antennas and Propagation (EuCAP 2018)*, pp. 1–5, London, UK, April 2018.

[15] IEEE Std 1528-2013 (Revision of IEEE Std 1528-2003), *IEEE Recommended Practice for Determining the Peak Spatial-Average Specific Absorption Rate (SAR) in the Human Head from Wireless Communications Devices: Measurement Techniques*, IEEE, 2013, https://search.library.wisc.edu/catalog/9912350582702121.

[16] P. A. Hasgall, F. Di Gennaro, C. Baumgartner et al., "IT'IS database for thermal and electromagnetic parameters of biological tissues," January 2015, http://www.itis.ethz.ch/database.

[17] N. Joachimowicz, C. Pichot, and J. P. Hugonin, "Inverse scattering: an iterative numerical method for electromagnetic imaging," *IEEE Transactions on Antennas and Propagation*, vol. 39, no. 12, pp. 1742–1753, 1991.

[18] Q. Fang, P. M. Meaney, S. D. Geimer, A. V. Streltsov, and K. D. Paulsen, "Microwave image reconstruction from 3-D fields coupled to 2-D parameter estimation," *IEEE Transactions on Medical Imaging*, vol. 23, no. 4, pp. 475–484, 2004.

[19] M. Polívka and D. Vrba, "Shielded micro-coplanar CRLH TL zeroth-order resonator antenna: critical performance evaluation," *Radioengineering*, vol. 18, no. 1, pp. 1592–1595, 2009.

[20] J. Vrba and D. Vrba, "A microwave metamaterial inspired sensor for non-invasive blood glucose monitoring," *Radioengineering*, vol. 24, no. 4, pp. 877–884, 2015.

[21] D. Vrba, J. Vrba, D. B. Rodrigues, and P. Stauffer, "Numerical investigation of novel microwave applicators based on zero-order mode resonance for hyperthermia treatment of cancer," *Journal of the Franklin Institute*, vol. 354, no. 18, pp. 8734–8746, 2017.

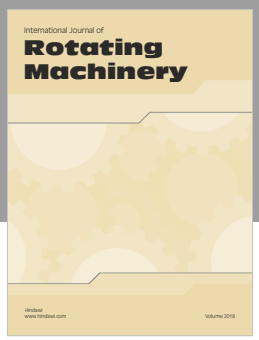

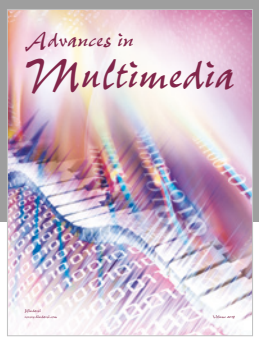

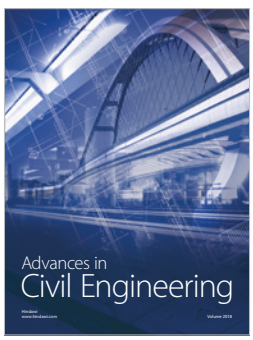

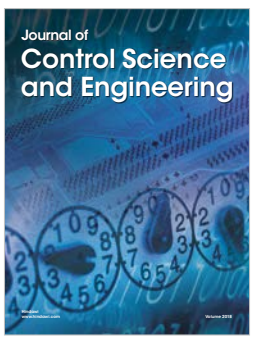

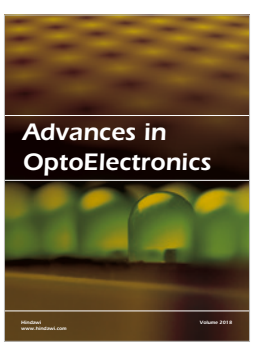

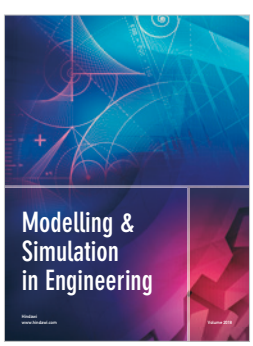

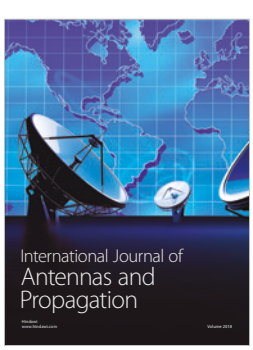

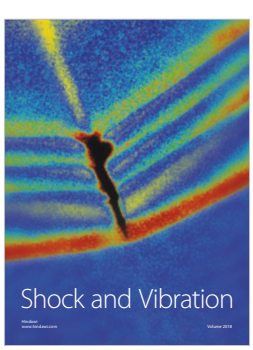

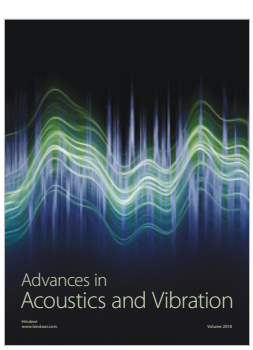

Hindawi

Submit your manuscripts at
www.hindawi.com